Hindawi
Wireless Communications and Mobile Computing
Volume 2022, Article ID 3735006, 19 pages
https://doi.org/10.1155/2022/3735006

Research Article

Simulation Calculation of the Collapse Process of High-Rise Steel Structure Energy-Forming Cutting Blasting Demolition

Xiaoguang Zhou

School of Mechanics and Civil Engineering, China University of Mining and Technology-Beijing, Beijing 100000, China

Correspondence should be addressed to Xiaoguang Zhou; bqd1800604041@student.cumtb.edu.cn

Received 19 March 2022; Revised 8 April 2022; Accepted 15 April 2022; Published 9 May 2022

Academic Editor: Chia-Huei Wu

The high-rise steel structure building (structure) is a relatively special structure. Due to its high height characteristics and the overall structure height and narrowness, there is still no unified method for this type of demolition. This paper is aimed at studying the simulation of the demolition of high-rise steel structures by blasting through computer video images. For this reason, this paper proposes a simulation of its specific blasting demolition work based on LS-DYNA software. Through an update to its core algorithm, it is more suitable for the simulation of this type of structure and simultaneously carried out simulation experiment research on the improved results. The experimental results of this paper show that the LS-DYNA software after the algorithm update is more referential to the simulation results of the simulation structure of high-rise steel structures. The simulation structure can increase the similarity to 97% in the actual demolition work, and the comparison probability of risks is also increased by nearly 31%. It can greatly improve the demolition problem of this kind of high-rise steel structure building (structure).

1. Introduction

As an important part of engineering blasting, disintegration blasting has gradually developed after World War II and has achieved brilliant results in the past 50 to 60 years. Using the dismantling blasting method to dismantle large and diverse buildings has become the best choice for dismantling projects. The theory of disintegration and blasting has also been continuously developed on this basis and has been improved. The demolition and blasting of frame structures, towering structures, foundations, bridges, etc. also have relatively mature calculation theories or experimental formulas and achieved good results in actual work. However, the explosive cracking of a part of a structure using a special structure is a stage in which empirical data obtained from engineering practice is used as the main design basis, and it needs to be improved.

In order to study the mechanical properties of high-rise steel structures, it is not enough to rely on empirical data alone. This article introduces a numerical method for simulating the collapse process widely used in the field of engineering. Using the unique stress cloud diagram and real-time animation function of the numerical simulation software, it intuitively describes the stress change and collapse process in the building explosion. This is very meaningful to support the design of blasting schemes. This numerical solution has been widely used in explosive cracking of high-rise buildings in recent years. Through multiple numerical simulations, specific structures are guided to select the most suitable blasting plan. The data actually collected after the explosion also proves that the prediction reliability of the numerical simulation method is very high. In high-rise steel structures such as prilling towers, in order to achieve a good blasting effect, numerical simulation software is used. It is very meaningful and promising to carry out computer simulation before determining the blasting plan and to predict the explosion effect intuitively and find the plan.

With the rapid development of China's infrastructure construction, many high-rise buildings have been erected, and many high-rise buildings are constantly being demolished and reconstructed. For the blasting demolition of steel structure buildings, the previous model is definitely no longer applicable. And this makes more and more people begin to invest in the simulation research of building blasting. Ainalis et al. pointed out that for a long time, the mining and construction industries have been facing considerable concern and criticism regarding the impact of blasting. Any increase in the explosion will generate ground vibration, which can spread over long distances and cause structural damage or discomfort to residential buildings in surrounding urban areas. In order to accurately predict the propagation of ground vibration near these sensitive areas, it is necessary to characterize and understand the blasting process and the surrounding environment [1]. Xie et al. used numerical simulation methods in his research to evaluate the reasons for the difficulties encountered in cutting and blasting. To overcome this difficulty, he adopted the Riedel-Hiermaier-Thoma (RHT) model in LS-DYNA software. In the simulation, the parameters of the RHT model are determined according to the existing experimental data, and the existing blasting experiments are used to verify the determined parameters of the RHT model. Finally, the RHT model is used to study the cutting blasting injury mechanism under different hydrostatic pressures and different lateral pressure coefficients [2]. Zhang et al. solved the problem of on-site measurement of the Excavation Damaged Zone (EDZ) and a numerical simulation method that simultaneously considered the effects of excavation unloading and blasting loads. He conducted a detailed analysis of the mechanical response of the actual measured data to the excavation and blasting rock mass. Subsequently, based on the findings of on-site measurement data, he proposed an EDZ determination numerical evaluation method that simultaneously considers the effects of excavation unloading and blasting loads [3]. Based on the Qifeng Mountain Tunnel of Zhengwan Railway, Wang et al. used field tests and three-dimensional dynamic numerical simulation methods to study the propagation law of cut-hole blasting vibration under the condition of axially uncoupled charges of air and water media and comparatively analyzed the attenuation characteristics of the vibration velocity of the main support at different distances and positions behind the working face [4]. Feng et al. passed the verification of the full-scale SERCEL impact test results and developed air gun impact test simulation technology for the design of the near-field non-explosive UNDEX test model scale. There is a highly advanced M&S (modeling and simulation) system using FSI (fluid structure interaction) analysis technology of LS-DYNA code for underwater blasting response analysis of full-scale air gun impact test and by comparing its impact characteristics and behavior with the results of the air gun impact test [5]. The first goal of Armaghani's research is to develop a flying rock estimation and prediction model based on multiple regression (MR) analysis and then use the developed MR model to simulate flying rock phenomena through the Monte Carlo (MC) method. In order to achieve his research goals, he investigated 62 blasting operations at the Ulu Tiram quarry in Malaysia and carefully recorded/calculated some controllable and uncontrollable factors. The obtained MC modeling results show that the method he studied can simulate the flying stone range with good accuracy [6]. The purpose of Ye's research is to develop and introduce new technologies to predict and simulate the flying rock phenomenon that occurs in the mine due to blasting. He has carried out the identification and measurement of important parameters affecting flying rocks in six different quarries in Malaysia and established an extensive database for various parameter studies of GP and RF models to obtain the best model [7]. In his research, Jayasinghe et al. used the coupled SPH-FEM method to study and quantify the response and possible damage of rock-socketed piles near the soil-rock interface underground impact excitation. The results show that the pile foundation is relatively fragile, and the nature of the soil has a significant influence on the response of the pile under a specific explosion load. In addition, based on the numerical results, he proposed the ground vibration attenuation equation (7). The abovementioned literatures have detailed introductions to blasting demolition, but most of the literatures explore the experimental part through actual experiments, and there are still too few simulation experiments. The research in this article is based on the LS-DYNA software to conduct simulation experiments on the blasting demolition of steel structures; so, a lot of simulation data is needed for research.

The innovation of this article is to conduct a practical investigation on the dismantling of the Red Square Pelletizing Tower of China Salt Hunan Zhuhua Group. After understanding its blasting and demolition work in detail, the LS-DYNA software is used to simulate its work, and the software algorithm (Lagrangian algorithm) is updated to make the simulation effect more referential. In the experiment and analysis part, it also analyzes the results of its simulation to improve its performance and analyze the improvement of the actual construction process.

2. Finite Element Analysis Method

2.1. Project Introduction. The Red Square Pelletizing Tower of Zhongyan Hunan Zhuhua Group has been in disrepair for a long time. For safety reasons, it was decided to demolish it by blasting. Because the steel structure has not been repaired for many years, the steel body is corroded, and occasionally, there will be debris falling, which brings great safety hazards to the construction safety. Before blasting, it is necessary to derust the periphery of the steel structure in the cut area to ensure the smooth formation of the cut [8].

2.1.1. Surrounding Environment. The steel structure to be dismantled (including the pelletizing tower, elevator shaft, and step ladder) is located next to the abandoned industrial plant. The northern part of the center point of the prilling tower is 165 m away from the office building; the houses in the area within 200 m of the northeast have been demolished, the eastern part is the factory fence and the residential

area outside the fence, and the closest distance to the blasting point is 140 meters; there is an inside road from north to south in the west, 137 m from the center of the tower; in the southwest, there is a 110 kV transmission line going from the southeast to the northwest with a vertical distance of 91.6 meters [9]. Due to the large number of surrounding buildings, there are few choices for the location of the collapse. After on-site environmental investigation, it was determined that the collapse direction of the prilling tower was set at 23° east by north. Before demolition by blasting, dismantle the factory buildings and uprights where the prilling tower has collapsed. According to the tender documents and on-site surveys, there are no pipelines and communication lines for the factory buildings and green spaces to be demolished under the collapsed area [10]. The schematic diagram of the surrounding environment of the prilling tower is shown in Figure 1.

2.1.2. Pelletizing Tower Structure. The prilling tower to be dismantled is a straight cylindrical steel structure with a height of 99.4 m. The side of the tower is supported by 24 vertical I-steel columns as columns, and the column spacing is 2.15 meters. A steel ring beam is installed every 1.8 m in the support column. U-shaped channel steel diagonal braces are set between the ring beam and the ring beam and between the ring beam and the support. The outer diameter of the ring beam is 17.1 m. Below ±0 is a reinforced concrete foundation with a buried depth of 8 m. The south side of the prilling tower is a steel structure square elevator and step ladder [11]. The structure of the steel structure is shown in Figure 2.

2.1.3. Engineering Requirements

(1) Ensure the construction period: adopt reasonable and advanced construction methods and strong technical measures to meet the construction period requirements proposed by the owner

(2) Ensure safety: accurately control the collapse direction of steel structures to ensure the safety of surrounding high-voltage lines, office buildings, and residential areas. Taking effective protective measures to reduce vibration and noise and strictly control the impact range of flying objects from shaped energy blasting; reduce the secondary flying stone hazard caused by the collision of steel structures on the ground; minimize the vibration of the prilling tower body impacting the ground; operate strictly in accordance with relevant regulations, strengthen safety measures, and ensure construction safety; and strengthen safety alert to ensure the safety of roads, buildings, and personnel and property near the explosion point [12]

(3) Ensure quality: meet the quality requirements of the owner

2.2. LS-DYNA Software. LS-DYNA is originated from DYNA3D of Lawrence Livermore National Laboratory in the United States. It was developed by J.O. Hallquist (elected as a member of the American Academy of Engineering in 2007) in 1976. In the early stage, it was mainly used for the stress analysis of the structure under impact load [13]. In the later stage, it was continuously updated to further standardize and improve the research results of DYNA. The application scope of DYNA program in the national defense and civil fields is expanded, the functions are enhanced, and a complete quality assurance system has been established [14].

The LS-DYNA program is a full-featured program for geometric nonlinearity (large displacement, large rotation and large strain), material nonlinearity (nearly 300 material dynamic models), and contact nonlinearity (nearly 100 types). It is based on the Lagrangian algorithm and has both ALE and Euler algorithms: mainly based on explicit solution, with implicit solution function; mainly structural analysis, combined with heat transfer, fluid, acoustics, electromagnetic, discrete element, chemical reaction, and multiphysics coupling functions; and mainly based on nonlinear dynamic analysis, with static analysis function. LS-DYNA is a general-purpose nonlinear multiphysics analysis program that combines military and civilian use [15]. The multiphysics coupling in LS-DYNA is shown in Figure 3.

Now, LS-DYNA has developed into the world's most famous universal multifunctional dynamic analysis program. It can simulate various complex problems in the real world and is especially suitable for solving explosions, rapid collisions, and various dimensional conflicts. Nonlinear dynamic impact problems such as metal forming can simultaneously solve the problems of heat transfer, fluid, sound, electromagnetic, chemical reaction, and fluid-solid combination [16]. Because the towering steel structure (structure) studied in this paper has a fast collapse rate and a high degree of nonlinearity, it is very suitable for LS-DYNA software to simulate its propagation law.

At present, in the field of steel structure building research, there are mainly three numerical simulation methods: finite element method, finite difference method, and finite volume method. Since this article mainly involves the introduction of the finite element method, it is only explained. Among them, the finite element method is the most commonly used [17–19]. It divides the continuous solution domain into multiple finite elements and forms a discrete model. Among them, LS-DYNA software is mainly used for the exploration of nonlinear problems such as blasting and building demolition. There are two main forms for solving similar values. One of them is structural finite element; the other is dynamic finite element. Among them, the application of finite element software LS-DYNA is the most common [20]. The steps for solving dynamic differentiation using LS-DYNA are as follows:

2.2.1. Pretreatment. Preprocessing mainly includes the following: setting preference options, selecting element types and algorithms, defining real constants, defining material properties, building solid models, meshing, creating PART, etc. [21].

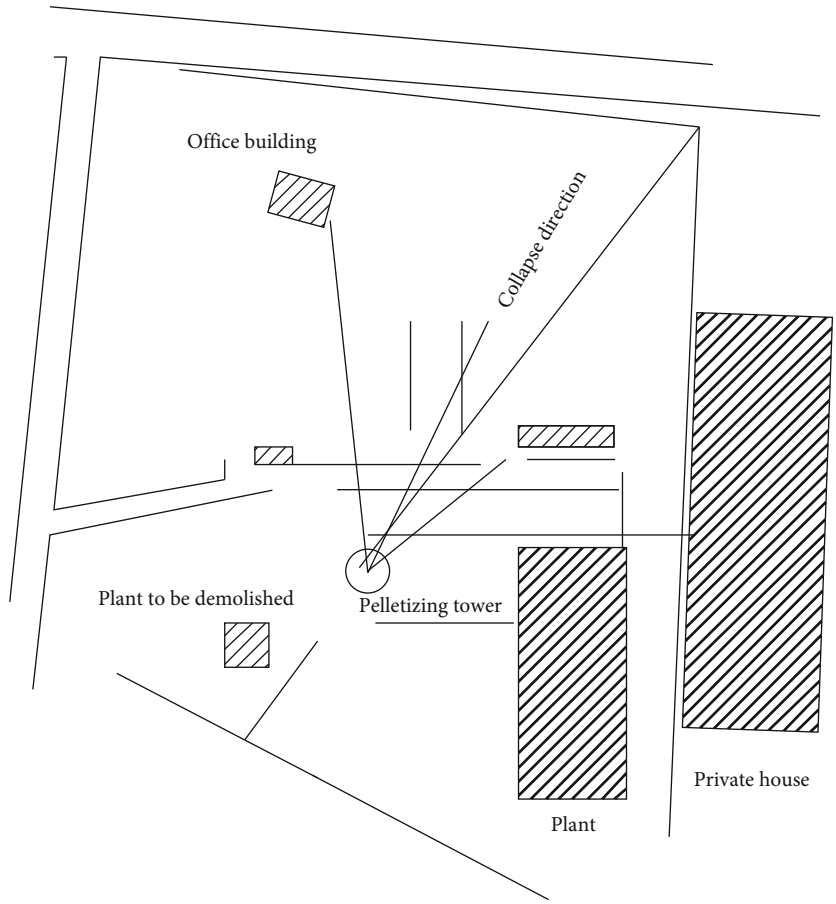

Figure 1: Schematic diagram of the surrounding environment of the prilling tower.

2.2.2. Loading and Solving. Loading and solving mainly include applying loads, constraints, boundary conditions, setting basic parameters, generating and outputting *K* files (file suffix k), and calling LS-DYNA for solving [22].

2.2.3. Postprocessing. Postprocessing is mainly to use ANSYS general postprocessor LS-PREPOST to read the calculation results of LS-DYNA and process the stress, strain, plastic strain, temperature, displacement, velocity, time history, and other curves [23].

2.3. Update Lagrangian Algorithm. Considering that the LS-DYNA program is based on the Lagrangian algorithm, and the algorithm capability of the Lagrangian algorithm in the LS-DYNA software occupies a relatively important proportion, so this article updates the Lagrangian algorithm [24]. The governing equation of the updated Lagrangian format consists of the following:

2.3.1. Mass Conservation Equation.

$$\rho(X,t)J(X,t) = \rho_0(X). \tag{1}$$

Momentum conservation equation is as follows:

$$\frac{\partial \sigma_{ij}}{\partial x_j} + \rho b_i = \rho ii_i. \tag{2}$$

Energy conservation equation is as follows:

$$\rho \dot{w}^{\text{int}_{ji_{ij}}}. \tag{3}$$

Deformation rate is as follows:

$$D_{ij} = \frac{1}{2}\left(\frac{\partial v_i}{\partial x_j} + \frac{\partial v_j}{\partial x_i}\right). \tag{4}$$

Constitutive relationship is as follows:

$$\sigma = \sigma\left(D_{ij}, \sigma_{ij}, \cdots\right). \tag{5}$$

Boundary conditions are as follows:

$$\begin{aligned} \left(n_j \sigma_{ji}\right)_A &= \overline{t_i}, \\ v_i|_A &= \overline{v_i}, \end{aligned} \tag{6}$$

(a) The overall view of the steel structure

(b) The bottom structure of the prilling tower

(c) Structure drawing of elevator and step ladder

Figure 2: Structural drawing of steel structure.

Initial conditions are as follows:

$$\dot{u}(X,0) = \dot{u}_0(X), \sigma(X,0) = \sigma_0(X), \tag{7}$$

$$\dot{u}(X,0) = \dot{u}_0(X), u(X,0) = u_0(X), \tag{8}$$

The actual situation of the problem requires that the momentum conservation equation is satisfied everywhere in the solution area, and it is almost impossible to solve this set of equations directly. The numerical algorithm starts from the weak form of the differential equation and only requires the momentum equation to satisfy in the sense of inner product. From this, the virtual power equation is derived, and after the finite element discretization, the node unique equation is obtained [25].

Taking the imaginary velocity as the weighting coefficient, using the weighted margin method, the weak form of the momentum equation can be written as

$$\int_v \delta v_j \left(\frac{\partial \sigma_{ij}}{\partial x_j} + \rho b_i - \rho \ddot{u}_i \right) dV = 0. \tag{9}$$

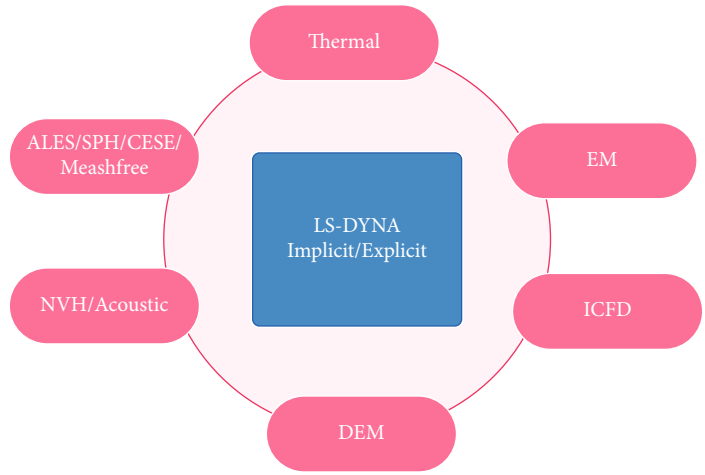

Figure 3: Multiphysics coupling in LS-DYNA.

In the formula, it is the virtual speed. Integrating the formula step by step, we can get

$$\int_v \frac{\partial(\delta v_i)}{\partial x_j}\sigma_{ji}dV - \int_v \delta v_i \rho b_i dV - \int_A \delta v_i \bar{t}_i dV + \int_v \delta v_i \rho \ddot{u}_i dV = 0. \tag{10}$$

The formula is the weak form of the momentum conservation equation and the surface force condition, which is called the virtual power equation. The solution is solved by the discretization of the finite element structure space, which can finally be written as the finite element ordinary differential equation format:

$$\mathrm{M}\ddot{\mathrm{U}} = F. \tag{11}$$

Solving the formula, the node displacement at the current moment can be obtained, and then the structural stress and strain can be obtained.

At the same time, in the solution of large deformation problems, the explicit analysis method with central difference time integration is mainly used [26]. This method can directly solve the control equations and eliminates the numerical iteration process in implicit analysis, which can save time and use resources. The acceleration vector of each node of the structural system at the end of the nth time step is calculated by Equation (11) as

$$\ddot{U}(t_n) = M^{-1}F. \tag{12}$$

Then, the node velocity and displacement vector are calculated by the following two formulas:

$$\begin{aligned} \ddot{U}(t_{n+1/2}) &= \dot{U}(t_{n-1/2}) + 0.5\,\ddot{U}(t_n)(\Delta t_{n-1} + \Delta t_n), \\ U(t_{n+1}) &= U(t_n) + \dot{U}(t_{n+1/2})\Delta t_n. \end{aligned} \tag{13}$$

The time step and time point in the formula are defined as

$$\begin{aligned} \Delta t_{n-1} &= (t_n - t_{n-1}), \\ \Delta t_n &= (\Delta t_{n+1} - t_n), \\ \Delta t_{n-1/2} &= 0.5(t_n + t_{n-1}), \\ \Delta t_{n+1/2} &= 0.5(t_{n+1} + t_n). \end{aligned} \tag{14}$$

Therefore, the new geometric configuration can be obtained by adding the displacement increment to the initial configuration, namely,

$$x_i(X_j, t + \Delta t) = x_i(X_j, 0) + u_i(X_j, t + \Delta t), i, j = 1, 2, 3. \tag{15}$$

Regarding the conditional stability of the explicit algorithm, the critical time step to ensure convergence must satisfy the following formula:

$$\Delta t \le \Delta t_{cr} = \frac{2}{\omega_n}. \tag{16}$$

ω_n is the highest natural vibration frequency of the system, and the eigenvalue equation of the smallest unit in the system is

$$\left|K^e - \omega^2 M^e\right| = 0. \tag{17}$$

The maximum eigenvalue obtained from this equation is ω_n. In order to ensure convergence, LS-DYNA adopts a variable step integration method, and the integration step at each moment is determined by the smallest element in the current configuration grid.

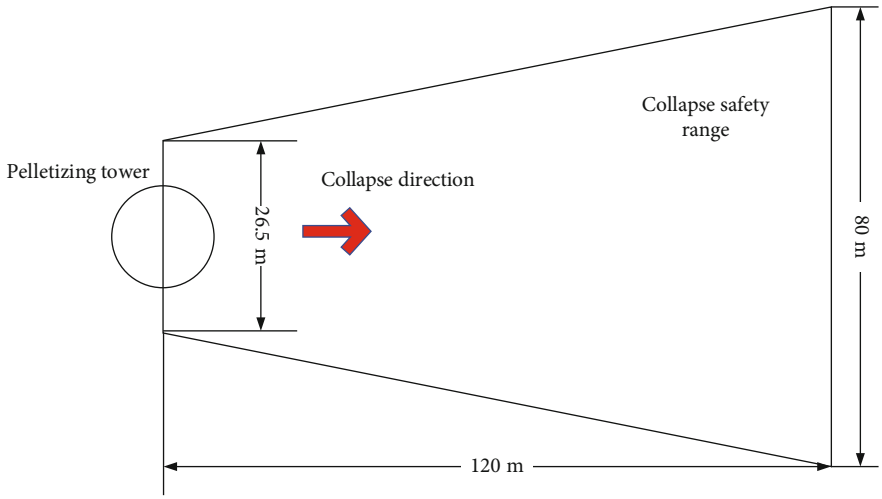

Figure 4: Schematic diagram of the safe collapse range of steel structures.

Table 1: Main construction equipment and equipment.

Serial number	Equipment name	Model and specification	Quantity	Country of origin	Throughput	For construction site	Remarks
1	/	Carter 320	2	U.S.A.	Good	Slag turning loading	/
2	Middle arm gun	Hitachi zx250	5	Japan	Good	Demolition fracture	/
3	Extended arm special High arm shear	Shengang 480	1	Japan	Good	Dismantle	/
4	High pressure waterwheel	Fire accident or sanitation vehicle	1 platform	Domestic	Good	Watering down dust	/
5	Oxygen cutting equipment	/	10 sets	Domestic	Good	Steel bar cutting	/
6	Walkie-talkie	/	15 sets	Domestic	Good	Command liaison	/
7	Protective equipment	/	Some	Domestic	Excellent	Protective envoy use	/
8	Emergency rescue vehicle	/	1 platform	Domestic	Excellent	First aid aid	/

3. Blasting Experiment of Steel Structure Building

3.1. Blasting Experiment

3.1.1. Design Principles. The basis of analyzing the blasting data of similar steel structure towering buildings at home and abroad sums up the past engineering practice experience of similar blasting of a company, combined with the characteristics of this project, it is safe, reliable and environmentally friendly [27].

3.1.2. Overall Plan. After on-site investigation, the surrounding environment of the steel structure is complex, there are many surrounding buildings, and there are few choices for the collapse position. After full discussion and demonstration by blasting experts, the following two solutions were proposed.

(1) Selection of Collapse Direction of Steel Structure.

(A) The collapse direction is 45° south to east. The advantages are: there is no building in this direction, no houses, and the site is open. Disadvantages are as follows: since there is a 110 kV line going from southeast to northwest in the south, when the steel structure collapses in this direction, it is greatly affected by the elevator steps. A slight angular deviation may affect the high-voltage line

(B) The collapsing direction is 23° east by north. Advantages are as follows: the field is open in this direction, the collapse distance is sufficient, and the collapse angle is less restricted. Disadvantages are as follows: there are private houses in this collapse direction, and the houses will be affected by the vibration of the collapse

After an on-site environmental survey by experts, it was finally determined that the direction of the collapse was 23°

east of north. The collapse vibration can be effectively reduced by excavating the damping ditch and constructing a strong barrier to reduce vibration and shock waves.

(2) Determination of the Overall Plan for the Collapse of the Steel Structure. The steel structure is self-heavy, the structure is complex, there are many steel components that need to be demolished by blasting at the cut, and the collapse site in the southeast direction is sufficient; so, the overall directional collapse is adopted.

According to the design standards, the requirements for the length of the steel structure in the collapse direction are site length $> (1.1 \sim 1.2)\, H = 120$ m.

In order to provide enough space for the collapse of the prilling tower and ensure the safety of collapse, the top two sides of the top of the collapse center line of the prilling tower are taken 40 m each, and the two sides of the bottom end are each taken from the buildings within the range of 4.7 m for predemolition as a safe space for the collapse of the prilling tower. The collapse safety range is shown in Figure 4.

(3) Directional Dumping Measures. Due to the surrounding environment restrictions, the collapse direction angle of the prilling tower requires strict control; so, the following dumping measures are adopted:

(1) Take an A-shaped blasting incision with accurate orientation

(2) Open a directional window in a trial explosion mode

(3) Use measuring instruments for precise positioning and determine the blasting location

(4) The blasting method uses shaped energy blasting to cut and dismantle the steel structure

(5) The combination of passive and active protection is adopted to strictly control the damage of the rebound rod of the energy-forming blasting, seismic waves, air shock waves, secondary splashes and ground vibrations, etc. Ensure the safety of surrounding buildings (structures), facilities, personnel, etc. that need to be protected

(6) Strictly organized, scientific, safe, and civilized construction

3.1.3. Pretreatment Work

(1) Deal with the ancillary facilities around the steel structure and predemolition the structures (factories) within the safe range of the collapse of the steel structure

(2) Cut and dismantle the connecting parts within the blasting incision range of the prilling tower, the two-layer funnel at the bottom of the prilling tower, auxiliary supports, and beams in the blasting incision

(3) Open a blasting directional window, customize a suitable shaped energy blasting cutter according to the experimental blasting, and cut off the support

(4) The ground vibration reduction measures in the direction of collapse are preset

(5) Before construction, the eccentric compression of the prilling tower was tested with theodolite, and the accurate collapsed central axis and cut position were identified

(6) Treat the surface of the steel structure to be cut

3.1.4. Main Construction Machinery Equipment Plan. The configuration of mechanical equipment can be flexibly deployed and supplemented within the company according to the actual conditions after construction. The construction equipment and equipment are shown in Table 1, and the construction network schedule is shown in Table 2.

3.2. Design of Blasting Parameters

(1) Cut form according to the structural characteristics of steel structure, comprehensive consideration of various factors such as construction, choose A-shaped mouth with accurate orientation. The bottom line of the cut is at the ground +1.4 m level

(2) The height of the cutout h is calculated based on the outer side of the support point where the center of gravity of the upper structure of the dismantled object is located in the dumping direction

$$(H -)\frac{\sqrt{H^2 - 2L^2}}{2 \le h}. \tag{18}$$

In the formula, L is the span between two external load-bearing supports, which is 2.5 m.

H is the height of the center of gravity of the superstructure, taking 49 m.

h is the height of the gap in m.

Calculate the height of the overturning disintegration gap according to the theory of collapse angle:

$$h = L \tan \varphi, \tag{19}$$

where L is the span between two external load-bearing supports, which is 2.5 m.

Φ is the collapse angle, which is 20°.

After calculation, $h = 2.5$ m.

In view of the large height of the prilling tower and most of the vertical I-beam supporting surface is rusted, experts have demonstrated that the height of the gap can be appropriately increased, and the maximum opening position is 9.3 m.

3.2.1. The Central Angle of the Incision. With reference to the conditions of demolition of high-rise concrete buildings by blasting and instability of high-rise buildings, the central

Table 2: Construction network schedule.

Serial number	Process name	Days 1-3	Days 4-6	Days 7-10	Days 11-14	Days 15-19	Day 20
1	Mobilization preparation: mobilization of personnel and equipment, erection of temporary facilities, erection of water and electricity pipelines, and handling of administrative permit for blasting operation	3 days					
2	Erection of predemolition platform		3 days				
3	Predemolition			4 days			
4	Shaped energy cutter, parameter determination, customization				4 days		
5	Arrange warning points, conduct the first explosion test, and cut off the directional window					5 days	
6	Install the shaped energy cutter according to the construction scheme						1 day
7	Protection, warning, and initiation						Same day as installation of shaped energy cutter
8	Crushing, garbage removal, and recovery						
9	Acceptance and demobilization						

Days 21-25.

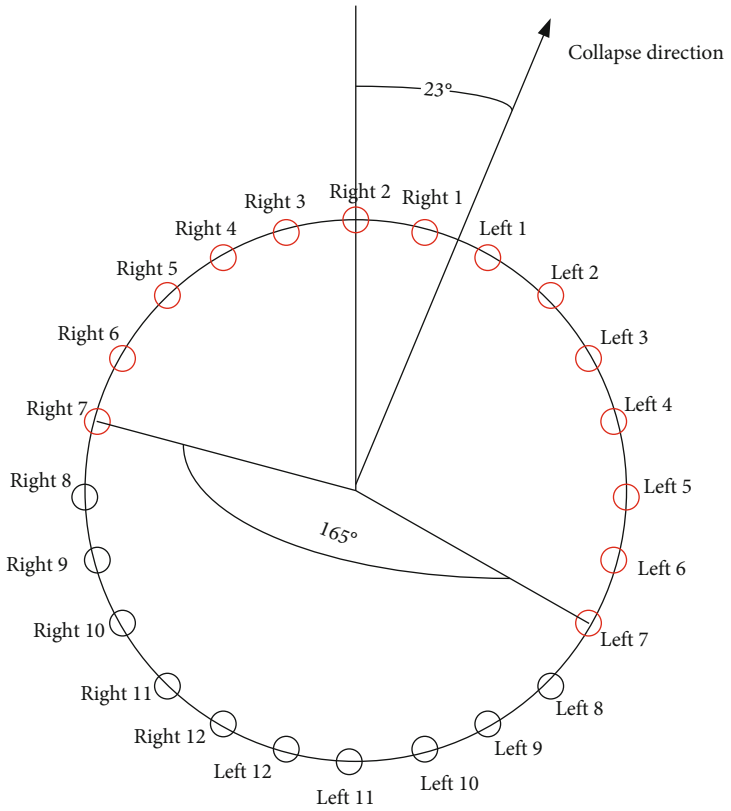

Figure 5: The central angle of the blasting gap of the prilling tower.

Figure 6: Before and after cutting the vertical support I-beam.

Table 3: Quantity of blasting equipment.

Material name	Specifications	Quantity	Remarks
Shaped energy cutter	200-250 g/m (RDX content)	70 rice	About 24 kg
Ordinary millisecond detonator (1 section)	Foot line length 10 m	200 hair	
Ordinary millisecond detonator (3 sections)	Foot line length 10 m	200 hair	
Ordinary millisecond detonator (5 sections)	Foot line length 10 m	200 hair	
Detonating cord		200 rice	
Detonating tube		3000 rice	

angle of the incision is 225°. The prilling tower needs to cut 14 support columns (left 1#-left 7#, right 1#-right 7# column). The central angle of the blasting notch of the prilling tower is shown in Figure 5.

3.2.2. Cutter Experiment. Experiment with the prefabricated cutter in the laboratory. The I-beam with thickness $\delta = 24$ mm, surface width $B = 0.8$ m, to carry out single-side cutting and two-side cutting. After arranging the cutting rope as required, the personnel were evacuated and detonated. After the explosion, the I-beam steel plates were cut, and the sections were neat.

At the same time, the I-beam has not been repaired for a long time on site. In order to reduce energy waste and noise pollution, single-sided cutting is adopted. The unilateral cutting effect of vertical support I-beam is shown in Figure 6.

3.2.3. The Amount of Blaster Used. The usage of the blaster is shown in Table 3.

3.2.4. Safety Distance for Ground Contact Vibration. For the blasting and demolition of high-priced buildings, we must pay attention to and check the vibration when it collapses. Generally, the collapse vibration is described by the vibration speed of the medium, and its vibration can be formally calculated:

Table 4: Collapse parameters of prilling tower.

Name	Pelletizing tower	Name	Pelletizing tower
M (t)	1000	H (m)	49.2
K_t	3.37	Σ (MPa)	10
G (m/s^2)	9.8	β	-1.66

The slumping vibration velocity is calculated by the following formula:

$$V_t = K_t \left(\frac{R}{(\mathrm{MgH}/\sigma)^{1/3}} \right)^{\beta}. \tag{20}$$

V_t is the ground vibration velocity caused by collapse, cm/s, and K_t is the attenuation coefficient.

According to the analysis of the blasting measured data of several high-rise buildings, the collapse vibration will be significantly reduced when the ground is excavated to reduce the vibration ditch, and the earth wall is built to change the ground contact condition of the building. kt generally takes 3.37. In this project, the buffer layer was laid. According to Zhou's "Discussion on the Calculation Formula of the Vibration Velocity of Blasting Demolition" from the

Table 5: Blasting letter mark table.

Signal type	Siren (whistle)	Instruction issuance	Main work
Advance signal	For the first time	Person in charge	Alert in place, traffic control
Initiation signal	The second time	Person in charge	Ignition initiation
Disarm signal	Third time	Person in charge	Alert evacuation

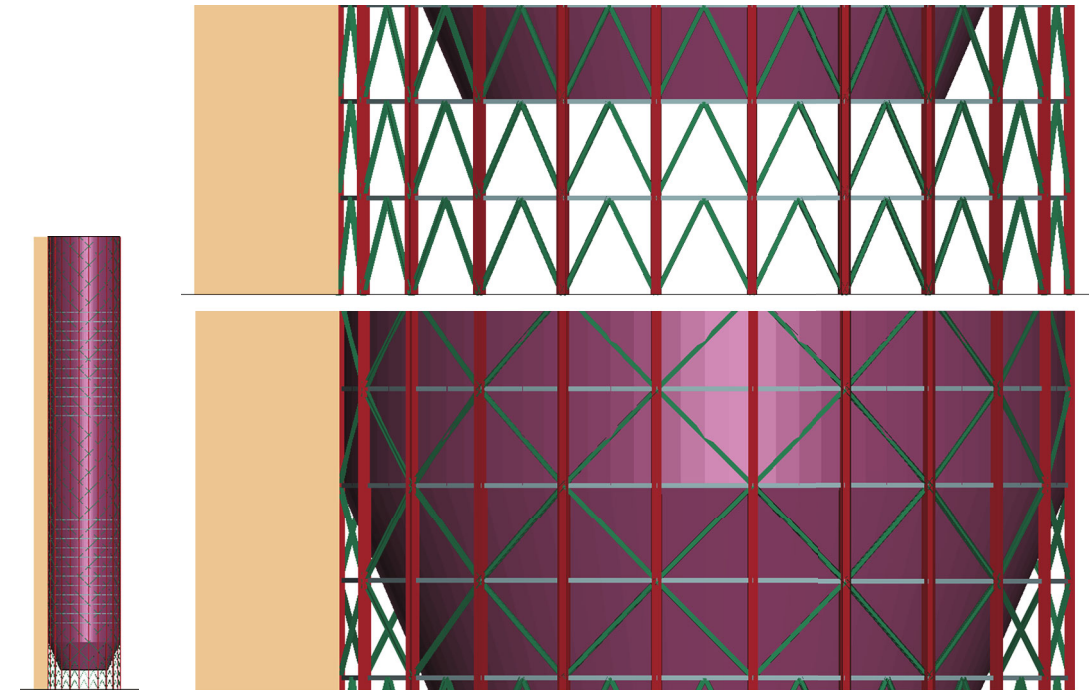

(a) Overall model (b) Partial model

Figure 7: Tower finite element model.

Institute of Mechanics of the Chinese Academy of Sciences, it was concluded that kt could be $3.37 \times 40\% = 1.348$.

M is the quality of the falling component, t, g-acceleration of gravity, m/s^2, H is the height of the center of gravity of the component, m, σ is the breaking strength of the ground medium, MPa, R is the distance from the observation point to the center of the impact ground, taking the distance from the nearest residential house to the center of the impact ground 115 m, and β is the slump vibration attenuation index, $\beta = -1.66 - 1.80$.

According to the site survey and drawings and data, the demolition value of the prilling tower is shown in Table 4.

3.2.5. Signal Regulation. The signal is a police siren.

The first signal is an alert.

This signal will be issued by the on-site commander after all preparations for blasting are completed, security personnel are in place, and personnel and vehicles within the cordon have been evacuated. After the warning signal was issued, the guards at each guard point further checked the evacuation situation, confirmed that there was no problem, and reported to the commander. The personnel at the ignition station ensure that the detonating circuit is kept in good condition and ready for ignition.

Second signal is the detonation.

After this signal is reported at each security point, the commander confirms that all personnel and vehicles within the security line have been evacuated. After the detonation signal was sent, the fireman at the ignition site charged immediately and reported to the commander of "charging completed" after completion. The commander then verbally issued the detonation command, the ignition hand pressed the button to detonate, and the two-person detonation was performed.

The third signal is lift the alert.

After the detonation, the blasting technicians quickly checked the blasting effect and reported to the commander when it was confirmed that there was no safety hazard. The commander issued a signal to lift the alert. After the dealert signal was issued, the personnel at the alert points withdrew and traffic resumed. The letter marking requirements for blasting are shown in Table 5.

3.3. Calculation Model Simulation. The finite element model of the tower is shown in Figure 7. Due to the large

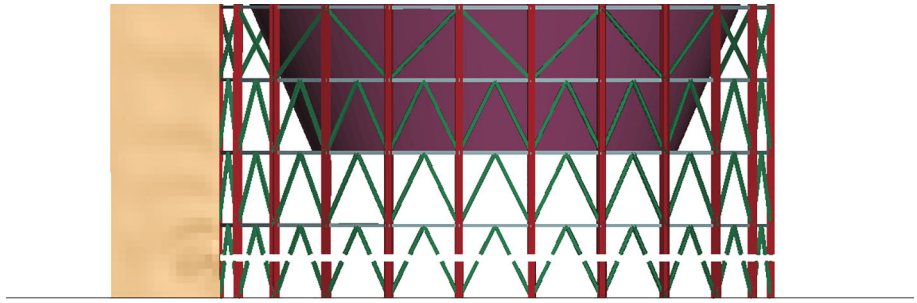

(a) 0.05 s cutting position

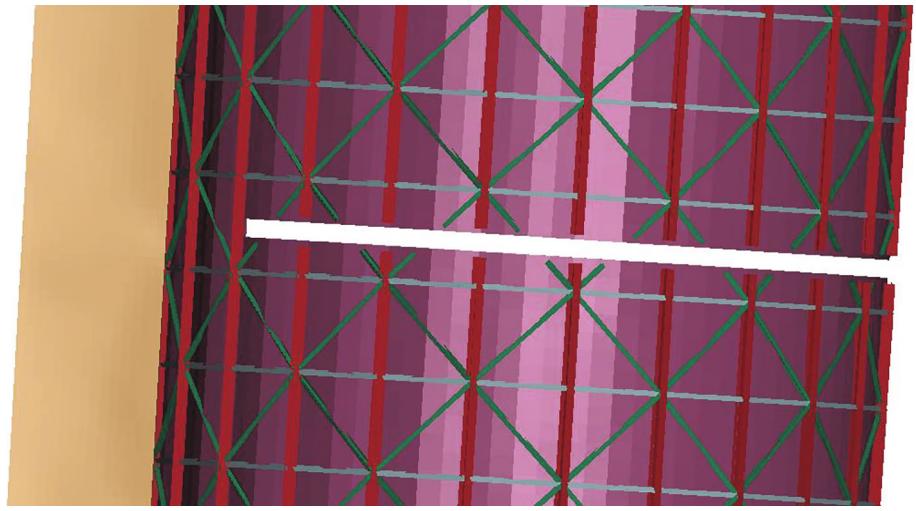

(b) 2 s cutting position

Figure 8: Tower cutting position.

size of the tower collapse calculation model and the long physical time for calculation, the calculation is very expensive. In order to reduce the calculation time, beam elements are used for I-beams, and shell elements are used for elevators and internal equipment. In order to reduce the calculation time, beam elements are used for I -beams, and shell elements are used for elevators and internal equipment. The ground is simplified by rigid walls, which can greatly reduce the calculation time, applying gravitational acceleration on the tower model.

Setting the bottom I-beam to cut off approximately 1 m from the ground at 0.05 s, as shown in Figure 8(a), cut off the structure and equipment at a distance of 63 m from the ground at 2 s, as shown in Figure 8(b).

The calculation software uses LS-DYNA. The tower adopts *MAT_PLASTIC_KINEMATIC material model. This is an elastoplastic material model with strain rate correlation and failure. The stress-strain relationship is approximately expressed by two straight lines. The slope of the first straight line is equal to the elastic modulus of the material, and the slope of the second straight line is the tangent modulus. The model can adopt isotropic hardening ($\beta = 1$), kinematic hardening ($\beta = 0$), or mixed hardening (($0 < \beta < 1$). The strain rate effect is described by the Cowper-Symonds model, and it is recommended to consider the viscoplastic strain rate effect (VP = 1).

*The relationship between the yield stress, plastic strain, and strain rate of the MAT_PLASTIC_KINEMATIC model is as follows:

$$\sigma_Y = \left(\sigma_0 + \beta E_p \varepsilon_p^{\text{eff}}\right)\left[1 + \left(\frac{\dot{\varepsilon}}{C}\right)^{1/P}\right]. \tag{21}$$

In the formula, σ_0 is the initial yield stress, $\dot{\varepsilon}$ is the strain rate, ε_p^{eff} is the effective plastic strain, β is the hardening parameter, E_p is the plastic hardening modulus, and C and P are strain rate parameters. The relationship between plastic hardening modulus E_p, elastic modulus E, and tangent modulus E_t (tangent modulus E_t cannot be less than zero or greater than the elastic modulus) is as follows:

$$E_p = \frac{EE_t}{E - E_t}. \tag{22}$$

4. Explosion Simulation Analysis

4.1. Simulation Results of Component Explosion Shock Wave Pressure

4.1.1. Simulation Results of Shock Wave Pressure in Air Medium. Curve A is the time-history curve of the head

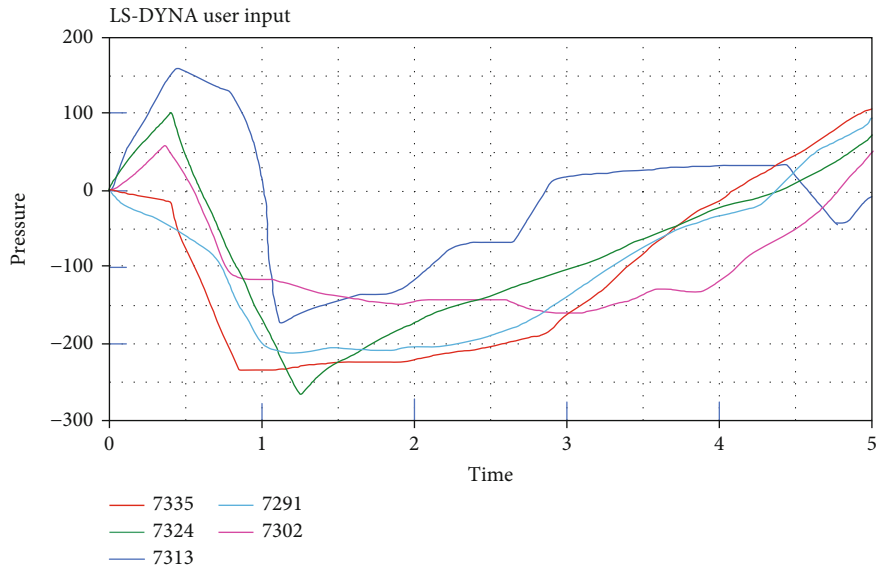

(a) Time history curve of typical unit pressure on the front surface of a round steel tube when exploded in air

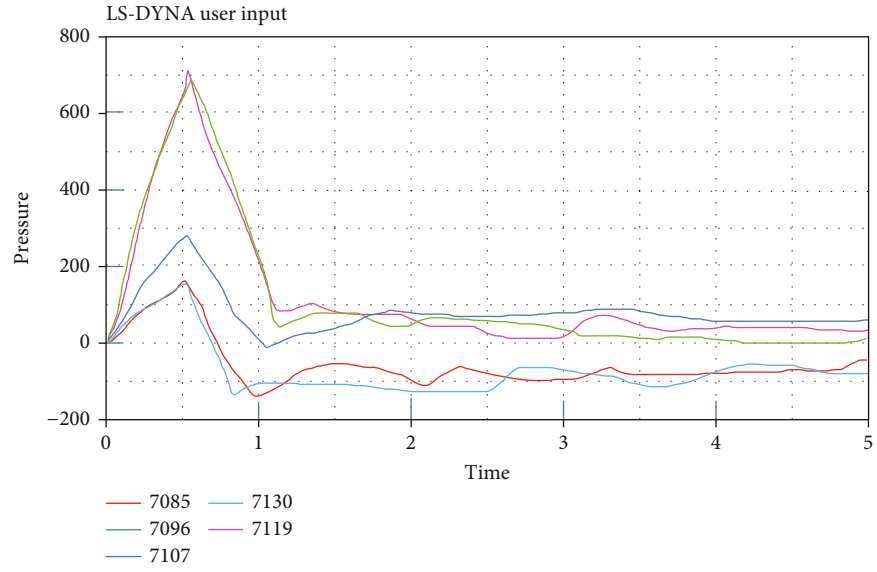

(b) Time history curve of typical unit pressure on the front surface of a round steel tube when exploded in air

Figure 9: Time-history curves of typical element pressure on the front surface of a round steel tube when exploded in two different media.

pressure on the head of unit 7335 at the bottom of the column, curve *B* is the time-history curve of the head pressure of the column 1/4 height of unit 7324, curve *C* is the time-history curve of the head pressure of unit 7313 in the middle of the column, curve *D* is the time-history curve of the head pressure of the column 3/4 height of unit 7302, and curve *E* is the time-history curve of the head pressure of unit 7291 at the top of the column. The simulation results of column pressure are analyzed.

The pressure time history curves of the five characteristic units of the explosion face are selected to represent the pressure changes of the explosion face at different heights. Generally speaking, the pressure at the detonating surface at each point in the time period of 0 ~ 0.5 ms is positive; in the 0.5 ~ 3.5 ms time period, the pressure at each point of the explosion face is negative pressure; within the period of 3.5 ms to 5 ms, the head pressure at each point is positive. On the whole, the central unit of the column has the highest pressure; units at 1/4 height and 3/4 height are followed by pressure; units at the top and bottom of the column have the least pressure. In each characteristic unit, the maximum value of positive pressure is 175 MPa, which occurs at 0.25 ms. The maximum negative pressure is 270 MPa, which occurs at 0.75 ms.

4.1.2. Simulation Results of Shock Wave Pressure in Soil Medium. Curve *A* is the time-history curve of the pressure on the head of unit 7086 at the bottom of the column; curve *B* is the time-history curve of the pressure on the head of unit 7096 at the height of column 1/4; curve *C* is the time-

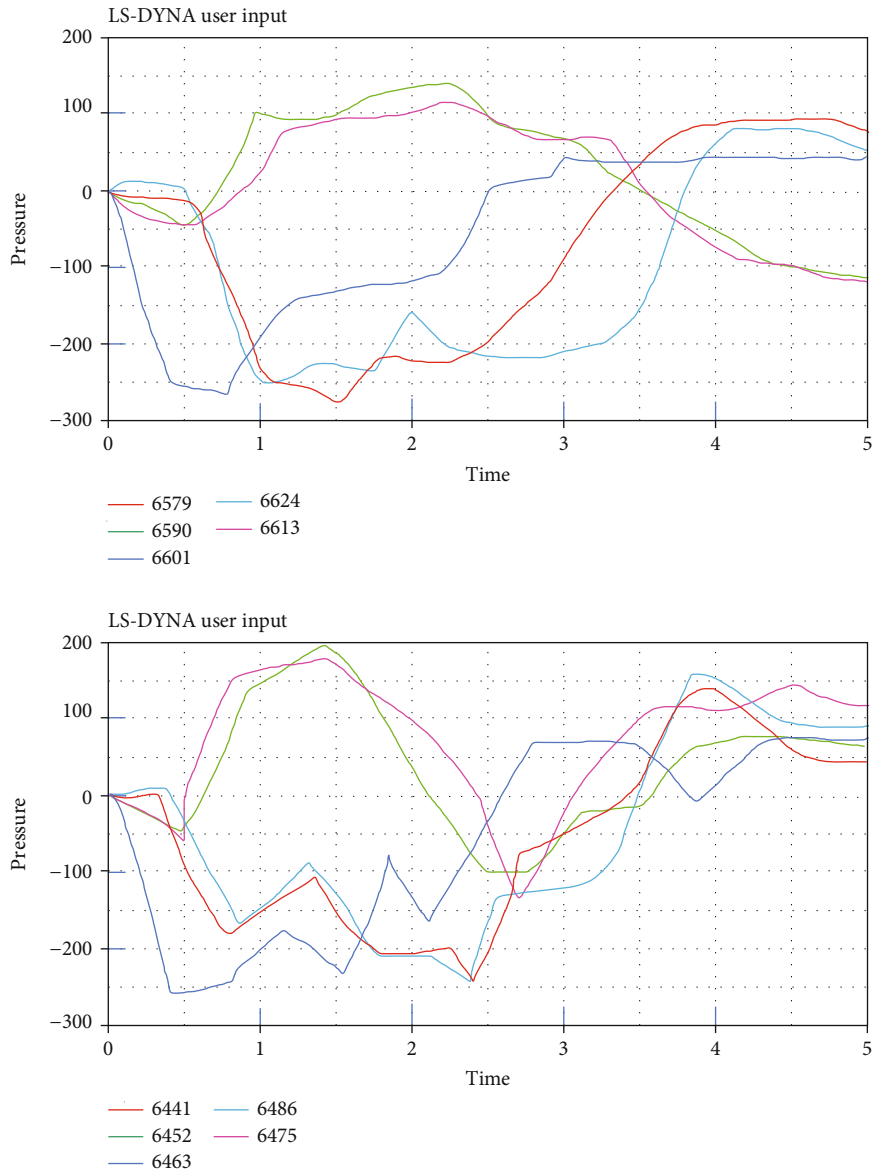

Figure 10: Time history curve of typical element pressure on the explosion face of steel pipes with different cross-sections during an explosion in the air.

history curve of the head pressure of unit 7107 in the middle of the column; the curve D is the time history curve of the head pressure of the 7130 unit at the height of column 3/4; curve E is the time history curve of the head pressure of No. 7119 unit at the top of the column. The simulation results of column pressure are analyzed.

From an overall point of view, the change trend of the pressure time history curve at each characteristic point is similar, and the pressure value tends to be stable after a complete half cycle. At 1/4 column height and 3/4 column height, the pressure value of the characteristic unit is greater than the pressure value of the characteristic unit in the column and the pressure value of the characteristic unit at the top and bottom of the column. The maximum positive pressure value is 700 MPa, which occurs at 0.25 ms. It occurs in characteristic units at 1/4 height and 3/4 height. The maximum negative pressure is 100 MPa, which occurs at the top and bottom of the column. It happens at various moments after 0.75 ms.

Different from the previous two media, the boundary condition of the rigid ground reflection has almost no effect on the pressure distribution of each point on the explosion face. The pressure distribution along the height direction of the burst face is highly symmetrical about the horizontal plane in the column. The pressure time history curves of the characteristic units at the top and bottom ends of the column are almost coincident, and the pressure time history curves at the height of 1/4 and 3/4 of the column are also nearly coincident. It illustrates the asymmetry of the boundary conditions at the top and bottom ends under the

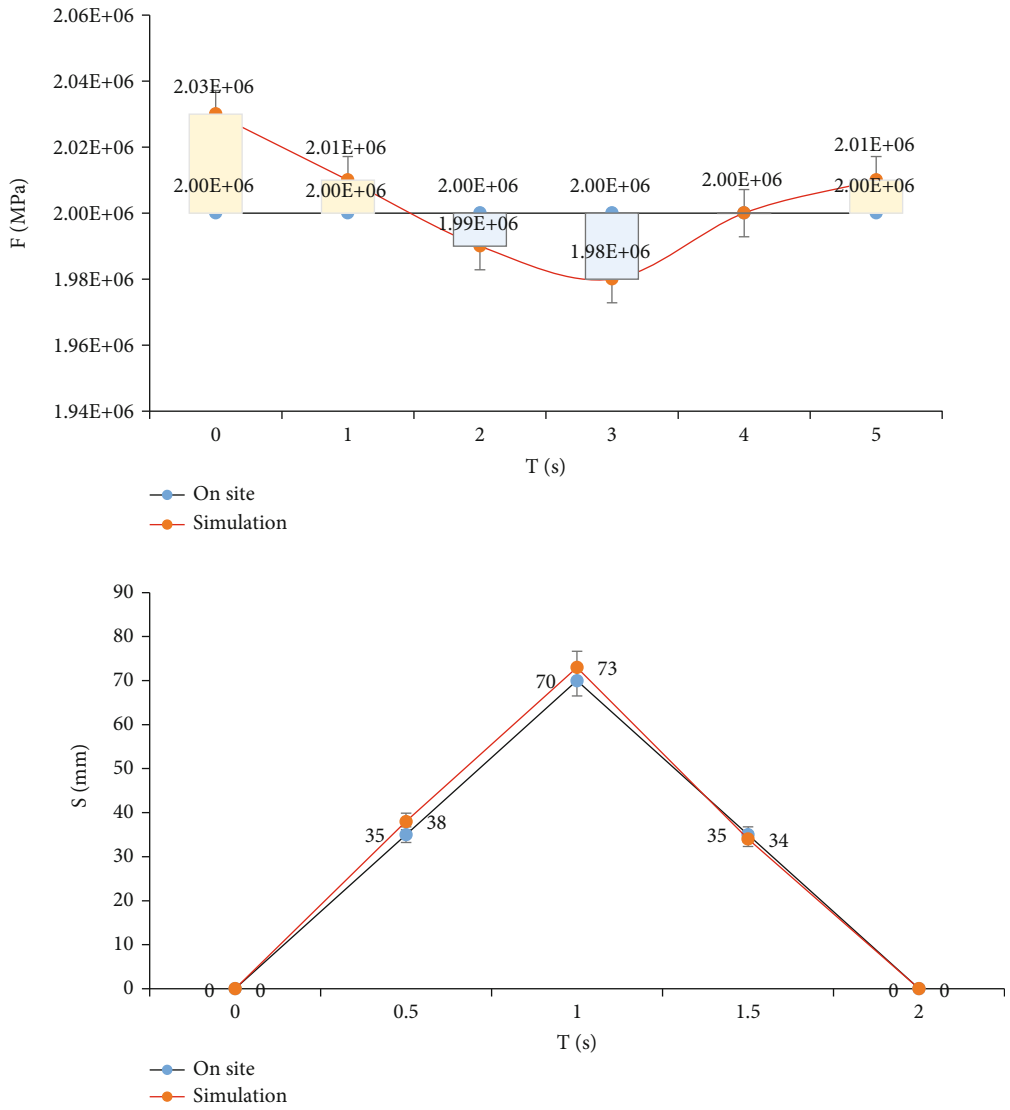

Figure 11: Force vs. displacement-time curve.

explosion load type selected in this paper. This has almost no effect on the stress distribution of the explosion-proof surface of the concrete-filled circular steel tube in the soil. The typical unit pressure time history curve diagram of the front surface of a round steel pipe when exploded in two different media is shown in Figure 9:

4.1.3. Analysis and Comparison of Shock Wave Pressure Simulation Results in Two Media. After comparing the pressure time history curves in two different media, the following conclusions are drawn:

(1) Comparison of the peak positive pressure on the explosive face of the components in the two media

The peak positive pressure of the explosive face of the component in the soil medium is the largest, which is much greater than the peak positive pressure of the medium in the air, and the peak positive pressure of the explosive face of the component in the air medium is the smallest.

(2) Comparison of the peak negative pressure on the explosive face of the components in the two media

The component in the air medium has the largest peak negative pressure on the explosion-facing surface, and the component in the soil medium has the smallest peak negative pressure on the explosion-facing surface.

(3) Comparison of the peak difference between the positive and negative pressures on the explosive face of the components in the two media

The component in the soil medium has the largest difference between the positive and negative pressure peaks on the explosion face, and the component in the air medium has

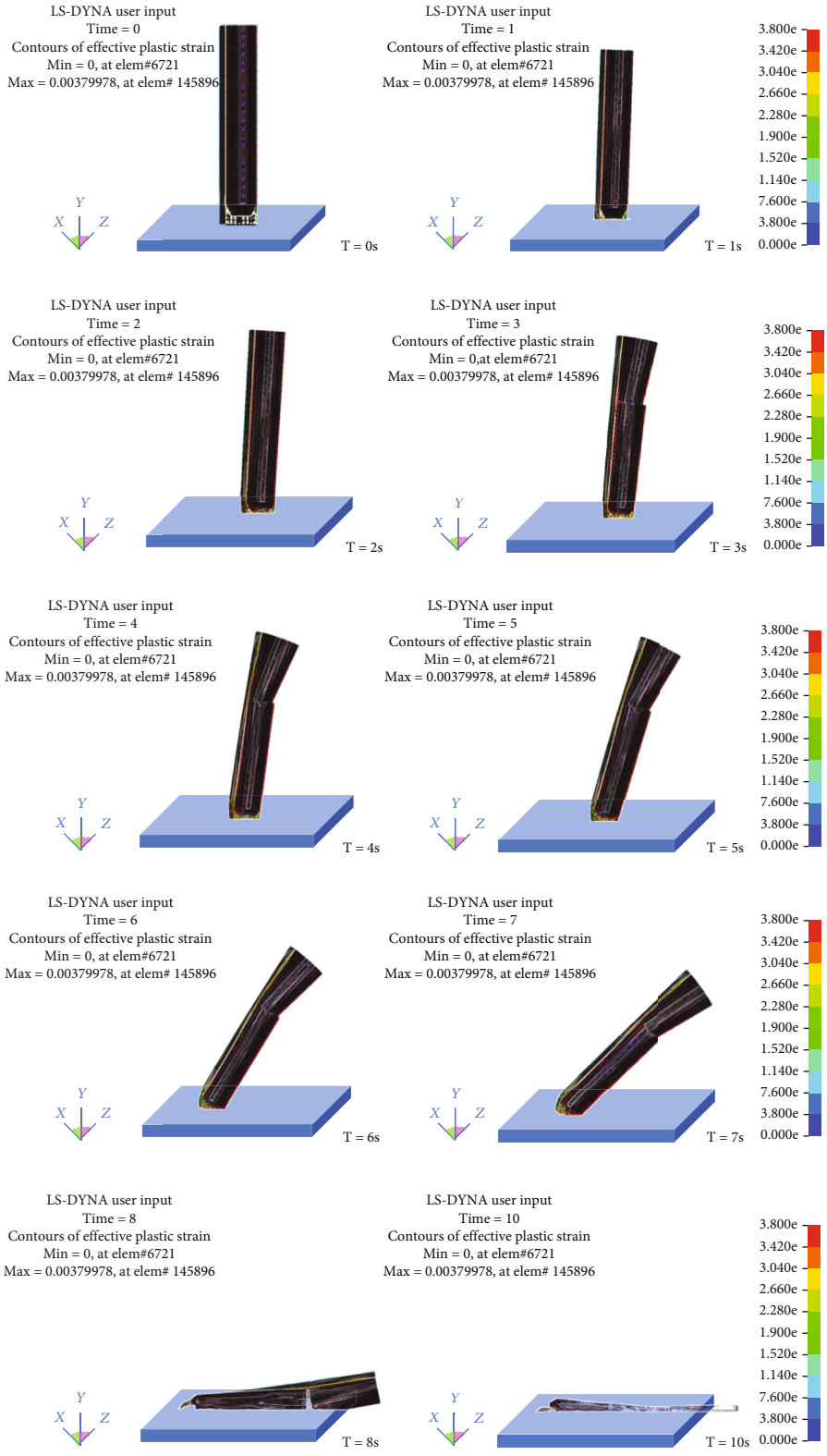

Figure 12: The collapse process of the tower.

Figure 13: Tower collapse range.

the smallest difference between the positive and negative pressure peaks.

(4) Comparison of the peak position of the positive pressure on the explosive face of the components in the two media

The peak of the positive pressure on the explosive face of the component in the air medium occurs at the middle of the column height, that is, at the position of 1/2 column height; the peak positive pressure on the explosive face of the component in the soil medium occurs at the position of 3/4 column height.

(5) Comparison of the peak position of the negative pressure on the explosive face of the components in the two media

The peak of the negative pressure on the explosion face of the component in the air medium occurs at the top of the column; the peak of the negative pressure on the explosion face of the component in the soil medium occurs at the top and bottom of the column almost simultaneously, and it is almost symmetric.

(6) Comparison of the influence of the restraint conditions at both ends of the top and bottom of the column on the pressure distribution on the explosion face of the two media

In the air medium, the constraint conditions at the top and bottom ends of the column are asymmetry. It will have a more obvious impact on the pressure distribution in the height direction of the explosive face and the pressure on the explosive face of the component presents an obvious asymmetric distribution; as for the soil medium, the constraint conditions at both ends of the top and bottom of the column are asymmetry. It has almost no effect on the pressure distribution in the height direction of the explosion face, and the pressure on the explosion face of the component is almost symmetrical.

(7) Comparison of the pressure change characteristics of the components in the two media

In the air medium, the change trend of the pressure time history curve of each characteristic unit at different heights is very similar, but the pressure peak is different, and there is a certain phase difference. The pressure time history curve of each characteristic unit can be summarized into four different stages according to the change trend: steep ascending section, steep descending section, slow ascending section, and stable section. In the soil medium, the change trend of the pressure time history curve of each characteristic unit at different heights is also very similar, but the pressure peak is different, and there is a certain phase difference. The pressure time history curve of each characteristic unit can be summarized into three different stages according to the change trend: steep ascending section, steep descending section, and slow descending (rising) section.

(8) The components in the two media have positive and negative pressures on the explosive face; so, the components need to consider symmetrical reinforcement

4.1.4. Analysis of Numerical Simulation Results of Explosion Shock Wave Pressure of Steel Pipe Members. Curve *A* is the time history curve of the pressure on the explosion face of unit 6579 at the bottom of the column, and curve *B* is the time history of the pressure on the explosion face of unit 6590 at the height of the column, curve *C* is the time history curve of the front pressure of unit 6601 in the middle of the column, curve *D* is the time history of the front pressure of unit 6624 at the height of the column, and curve *E* is the time history of the pressure of unit 6613 at the top of the column, analyzing the column pressure simulation results.

The maximum positive pressure value is 220 MPa, which occurs at 1.5 ms and at 1/4 column height unit; the maximum negative pressure value is 285 MPa, which occurs at the characteristic unit in the 0.5 ms column.

It is worth noting that the maximum negative pressure value is actually greater than the maximum positive pressure value. This inspires us that for load-bearing components that may be subjected to explosive loads, the cross-sectional form of the component should be designed to be symmetrical as much as possible. When exploded in the air, the typical unit pressure time history curve of the explosion face of different cross-section steel pipes is shown in Figure 10.

After comparing the pressure time history curves of two different cross-section steel pipes, the following conclusions are drawn:

(1) Comparison of the peak positive pressure on the explosion face of the equal-material square steel tube

and the equal-diameter square concrete-filled steel tube column

The peak value of the positive pressure on the explosion face of the equal material square steel tube concrete column is the largest, and the peak of the positive pressure on the explosion face of the equal diameter square steel tube column is smaller.

(2) Comparison of the peak negative pressure on the explosion face of the equal-material square steel tube and the equal-diameter square concrete-filled steel tube column

The peak value of the negative pressure on the explosion face of the equal material square steel tube column is the largest, and the peak of the negative pressure on the explosion face of the equal diameter square steel tube column is slightly smaller than that of the equal material square concrete filled steel tube column.

(3) Comparison of the peak difference between the positive and negative pressures of the equal-material square steel tube and the equal-diameter square concrete-filled steel tube column

The peak difference between the positive and negative pressure on the explosion face of the equal-material square steel tube concrete column is the largest, and the peak difference between the positive and negative pressure on the explosion face of the equal-diameter square steel tube column is small.

4.2. Apply Load and Define Constraint Analysis. Unlike many implicit analyses, all loads in an explicit analysis must be related to time. A vertical load of 2 MPa is applied to the top section of the column. The displacement of the column top applied in this paper is also applied in the form of load. The force vs. displacement-time curve is shown in Figure 11.

Because the bottom of the column in this model is a fixed end, the freedom of movement in the X, Y, and Z directions of the nodes on the bottom of the column is constrained, and the displacement of all nodes at the bottom of the column is restricted. At the same time, it combines the degrees of freedom of all nodes in the top section of the column on the Z axis.

4.3. The Finite Element Calculation Simulation Results and Analysis of the Collapse Process. Set the cut area in the tower at a predetermined time. The collapse process of the tower is shown in Figure 12. The tower collapsed at 10 s, and the collapse range is shown in Figure 13: the main direction is 102.4 m, and the lateral direction is 23.7 m.

From the results of the finite element calculation and simulation of the two collapse processes above, we can perform a good simulation process of the collapse process of the prilling tower, to understand the changes in the shape of the prilling tower during the collapse process and to avoid the risks in the actual construction process. After simulation, the risk aversion rate for the actual demolition of high-rise steel structures can be increased by 31%. The coincidence rate of the actual collapse and the simulated structure during the demolition process was increased to 97%, which greatly improved the difficulty of construction for the actual building demolition work.

5. Conclusions

This article mainly studies the simulation of blasting demolition of high-rise steel structures under computer video images. Through the use of LS-DYNA software, the staff can perform a simulation of its blasting demolition work on the computer, so that we can have a specific understanding of the demolition work, and at the same time, through the update and improvement of the Lagrangian formula in the technical aspect, so that the improved Lagrangian formula in LS-DYNA can be more suitable for the subject of this paper, making the simulation level higher and more in line with actual construction requirements.

Data Availability

The data that support the findings of this study are available from the corresponding author upon reasonable request.

Conflicts of Interest

The author declared no potential conflicts of interest with respect to the research, authorship, and/or publication of this article.

References

[1] D. Ainalis, O. Kaufmann, J. P. Tshibangu, O. Verlinden, and G. Kouroussis, "Modelling the source of blasting for the numerical simulation of blast-induced ground vibrations: a review," *Rock Mechanics & Rock Engineering*, vol. 50, no. 1, pp. 1–23, 2016.

[2] L. X. Xie, W. B. Lu, Q. B. Zhang, Q. H. Jiang, M. Chen, and J. Zhao, "Analysis of damage mechanisms and optimization of cut blasting design under high in-situ stresses," *Tunnelling & Underground Space Technology*, vol. 66, pp. 19–33, 2017.

[3] Y. Zhang, X. Ding, S. Huang, Y. Qin, P. Li, and Y. Li, "Field measurement and numerical simulation of excavation damaged zone in a 2000 m-deep cavern," *Geomechanics and Engineering*, vol. 16, no. 4, pp. 399–413, 2018.

[4] L. Wang, X. Zhang, M. Ma, J. Chen, and Z. Xu, "3D numerical simulation of tunnel blasting vibration laws under axial uncoupled charge with water medium," *Modern Tunnelling Technology*, vol. 55, no. 2, pp. 96–102, 2018.

[5] C. Feng, S. H. Li, W. H. Hao, and W. Ge, "Numerical simulation for penetrating and blasting process of EPW based on CDEM," *Journal of Vibration and Shock*, vol. 36, no. 13, pp. 11–18, 2017.

[6] D. J. Armaghani, A. Mahdiyar, M. Hasanipanah, R. S. Faradonbeh, M. Khandelwal, and H. B. Amnieh, "Risk assessment and prediction of Flyrock distance by combined multiple regression analysis and Monte Carlo simulation of quarry blasting," *Rock Mechanics and Rock Engineering*, vol. 49, no. 9, pp. 3631–3641, 2016.

[7] J. Ye, M. Koopialipoor, J. Zhou, D. J. Armaghani, and X. He, "A novel combination of tree-based modeling and Monte Carlo simulation for assessing risk levels of flyrock induced by mine blasting," *Natural Resources Research*, vol. 30, no. 1, pp. 225–243, 2021.

[8] R. Yang, C. Ding, L. Yang, Z. Lei, and C. Zheng, "Study of decoupled charge blasting based on high-speed digital image correlation method," *Tunnelling and Underground Space Technology*, vol. 83, pp. 51–59, 2019.

[9] C. Collins, K. R. Fister, B. Key, and M. Williams, "Blasting neuroblastoma using optimal control of chemotherapy," *Mathematical Biosciences & Engineering*, vol. 6, no. 3, pp. 451–467, 2017.

[10] T. B. B. M. C. M. R. X. Yu, "Lecture notes in computer science image and video technology," *Adaptive Window Strategy for High-Speed and Robust KLT Feature Tracker*, vol. 9431, pp. 355–367, 2016.

[11] M. Paul, C. Hitoshi, and Q. Huang, "Lecture notes in computer science image and video technology," *Multi-Objective Visual Odometry*, vol. 10749, pp. 62–74, 2018.

[12] Y. Zhao, X. Kong, and D. Taubman, "A QoE-aware video quality guarantee mechanism in 5G," in *International Conference on Image and Graphics*, vol. 30, pp. 336–352, Springer, Cham, 2017.

[13] S. Satoh, "Lecture notes in computer science image and video technology," *Crowd Counting from a Still Image Using Multi-scale Fully Convolutional Network with Adaptive Human-Shaped Kernel*, vol. 10799, pp. 227–240, 2018.

[14] T. C. Li, H. Zhang, Z. G. Zhang et al., "Deep hole pre-splitting blasting technology when fully mechanized coal mining face passes through high drop fault," *Journal of the China Coal Society*, vol. 44, no. 1, pp. 199–209, 2019.

[15] H. C. Zhai, F. Y. Ren, and S. Q. Nan, "Stage blasting Technology of Large and Thick Steeply Inclined Orebody," *Journal of Northeastern University*, vol. 38, no. 10, pp. 1486–1490, 2017.

[16] E. Deng, W. Yang, and P. Zhang, "Analysis of surrounding rock vibration and the influence of soft rock mechanical parameters during the tunnel blasting with thin bedrock roof," *Geotechnical and Geological Engineering*, vol. 38, no. 1, pp. 537–550, 2020.

[17] B. Wang, B. F. Zhang, X. W. Liu, and F. C. Zou, "Novel infrared image enhancement optimization algorithm combined with DFOCS," *Optik*, vol. 224, article 165476, 2020.

[18] H. Song and M. Brandt-Pearce, "A 2-D discrete-time model of physical impairments in wavelength-division multiplexing systems," *Journal of Lightwave Technology*, vol. 30, no. 5, pp. 713–726, 2011.

[19] Y. Huang, W. Sheng, P. Jin, B. Nie, M. Qiu, and G. Xu, "A node-oriented discrete event scheduling algorithm based on finite resource model," *Journal of Organizational and End User Computing (JOEUC)*, vol. 31, no. 3, pp. 67–82, 2019.

[20] Z. Yahui, Z. Qixiao, Z. Wangfei, F. Song, S. Shuxian, and F. Jianing, "Techniques for analyzing data of multi-blasting points tested with video theodolite," *Journal of Applied Optics*, vol. 37, no. 2, pp. 209–214, 2016.

[21] S. G. Lee, J. S. Lee, J. H. Park, T. Y. Jung, H. S. Lee, and K. H. Park, "Verification of underwater blasting response analysis of air gun using FSI analysis technique," *Journal of the Society of Naval Architects of Korea*, vol. 54, no. 6, pp. 522–529, 2017.

[22] S. Zeng, S. Wang, B. Sun, and Q. Liu, "Propagation characteristics of blasting stress waves in layered and jointed rock caverns," *Geotechnical and Geological Engineering*, vol. 36, no. 3, pp. 1559–1573, 2018.

[23] H. Chu, X. Yang, S. Li, and W. Liang, "Experimental study on the blasting-vibration safety standard for young concrete based on the damage accumulation effect," *Construction and Building Materials*, vol. 217, pp. 20–27, 2019.

[24] S. Y. Xiao, L. J. Su, Y. J. Jiang, and Z. X. Liu, "Numerical analysis of hard rock blasting unloading effects in high in situ stress fields," *Bulletin of Engineering Geology & the Environment*, vol. 78, no. 2, pp. 867–875, 2019.

[25] J. H. Yang, C. Yao, Q. H. Jiang, W. B. Lu, and S. H. Jiang, "2D numerical analysis of rock damage induced by dynamic in-situ stress redistribution and blast loading in underground blasting excavation," *Tunnelling & Underground Space Technology*, vol. 70, pp. 221–232, 2017.

[26] J. Zhou, W. Lu, P. Yan, M. Chen, and G. Wang, "Frequency-dependent attenuation of blasting vibration waves," *Rock Mechanics & Rock Engineering*, vol. 49, no. 10, pp. 4061–4072, 2016.

[27] Z. Xu, Y. Xie, K. Zhang, Y. Hu, X. Zhu, and H. Shi, "Design and optimization of a magnetic wheel for a grit-blasting robot for use on ship hulls," *Robotica*, vol. 35, no. 3, pp. 712–728, 2017.